Magnetic Resonance Imaging 44 (2017) 55–59

Contents lists available at ScienceDirect

Magnetic Resonance Imaging

journal homepage: www.mrijournal.com

Original contribution

# Simple algorithm for the correction of MRI image artefacts due to random phase fluctuations☆

Lionel M. Broche *, P. James Ross, Gareth R. Davies, David J. Lurie

*Aberdeen Biomedical Imaging Centre, School of Medicine and Dentistry, University of Aberdeen, Scotland, UK*

ARTICLE INFO

*Article history:*
Received 22 May 2017
Accepted 23 July 2017
Available online xxxx

*Keywords:*
Fast field-cycling MRI
Phase encode artefact
Correction algorithm
Post-processing

ABSTRACT

*Purpose:* Fast Field-Cycling (FFC) MRI is a novel technology that allows varying the main magnetic field $B_0$ during the pulse sequence, from the nominal field (usually hundreds of millitesla) down to Earth's field or below. This technique uses resistive magnets powered by fast amplifiers. One of the challenges with this method is to stabilise the magnetic field during the acquisition of the NMR signal. Indeed, a typical consequence of field instability is small, random phase variations between each line of k-space resulting in artefacts, similar to those which occur due to homogeneous motion but harder to correct as no assumption can be made about the phase error, which appears completely random. Here we propose an algorithm that can correct for the random phase variations induced by field instabilities without prior knowledge about the phase error.

*Methods:* The algorithm exploits the fact that ghosts caused by field instability manifest in image regions which should be signal free. The algorithm minimises the signal in the background by finding an optimum phase correction for each line of k-space and repeats the operation until the result converges, leaving the background free of signal.

*Conclusion:* We showed the conditions for which the algorithm is robust and successfully applied it on images acquired on FFC-MRI scanners. The same algorithm can be used for various applications other than Fast Field-Cycling MRI.



## 1. Introduction

Fast Field-Cycling (FFC) is a technique that involves varying the main magnetic field $B_0$ during the pulse sequence. The term 'Fast' indicates that the duration of the transition between two fields is much shorter than the typical $T_1$ value of the sample investigated so that one can measure the field-dependence of the relaxation rate of a sample and infer information about its structure [2–6]. Our research team is interested in translating FFC into MRI to exploit the high information content it provides for *in vivo* medical applications [7], as well as to exploit field-localised effects as contrast mechanisms [8,9].

Cartesian MRI acquisitions rely on the magnetic field stability in order to maintain the phase information across k-space. This may be a problem in noisy environments, for instance with the proximity of elevators or roads, or when motion occurs during the scan. It is even more of a challenge for FFC-MRI scanners as field control for resistive system depends on their inductive load and FFC requires small inductance in order to obtain responsive magnets [1]. For instance our whole-body FFC-MRI resistive magnet has an inductance of 55 mH and must reach 0.2 T in 20 ms, corresponding to a slew rate of 10 T/s, with a stabilisation time of 20 ms before acquisition, while our pre-clinical FFC-MRI scanner is more compact and can reach 0.5 T in a similar time. Magnetic field stability is a problem on both systems and we observe ghosting in the phase-encode direction after image reconstruction, reminiscent to motion artefacts. Short acquisition techniques such as ZTE could be used to mitigate this problem but they require strong gradient amplifiers and fast switching RF coils. Additionally, the minimum echo time allowed by our gradient amplifiers is of the order of 10 ms which is enough to build up significant random dephasing so that techniques such as navigator images [10] are not possible, since the information on the phase error is lost between the navigator data and the image echo. One could measure the field fluctuations and deduce the phase corrections to apply to the image but that requires a fast field probe with sensitivity of the order of a ppm at a nominal field of 200 mT, which we do not currently have.

Therefore a post-processing correction technique is required. The algorithm presented here is a simple post-processing technique both in k-space and image space, inspired from motion correction algorithms [11,12], that allows robust correction of the artefact observed in FFC-MRI

☆ Grant support: This work was supported by EPSRC [grant numbers EP/E036775/1, EP/K020293/1] and received funding from the European Union's Horizon 2020 research and innovation programme [grant agreement No 668119, project "IDentIFY"].

* Corresponding author at: Biomedical Physics Building, Foresterhill, Aberdeen, AB25 2ZD, UK.
*E-mail address:* l.broche@abdn.ac.uk (L.M. Broche).

http://dx.doi.org/10.1016/j.mri.2017.07.023

and allows characterising the phase variations at the post-processing stage at the cost of oversampling over a signal-free region. It takes advantage of the fact that random phase errors between k-space lines lead to a smear across the entire image so that signal-free regions only show ghosting.

## 2. Methods

### 2.1. Correction algorithm

The algorithm developed here focuses on acquisitions made using Cartesian k-space sampling. It is structured by two iterative loops: one that minimises the background signal and another that estimates the background and tests for convergence (Fig. 1). The initial image is first reconstructed by inverse fast Fourier transform and segmented into a background and an object by thresholding on the magnitude image. At that point the background is coarsely estimated because of the smear in the phase-encode direction. Initial guesses for the background may be added, if provided by the user. The algorithm then estimates the phase corrections for all the phase-encoded k-space lines using a sequential quadratic programming (SQP) method [13]: at each iteration the phase errors are estimated, the image is reconstructed with the estimated phase correction and the amount of signal in the background is extracted for use as a minimisation criterion. When an acceptable estimation of the phase error is obtained the algorithm estimates the background from the new corrected image and tests for convergence compared to the previous estimation of the background. If the variation between the new phase error estimation and its previous value is greater than a threshold then the algorithm re-estimates the background using the best corrected image and re-iterates the phase estimation loop. We added some constraints on the SQP search so as to null the 1st order moment of the phase correction array in order to avoid translation of the image in the phase-encode direction. We also constrained the average correction phase to zero to speed up the convergence since this parameter does not affect the outcome of the algorithm. Finally, we tested the algorithm either with or without an estimation of a signal-free region added to the estimated background at the first iteration. The algorithm was programmed using Matlab 2014a (Mathworks, Natick MA USA).

### 2.2. Reconstruction of simulated data

The algorithm was first tested for robustness by Monte-Carlo methods. A 128 × 128 gradient echo image of a phantom previously acquired on a stable MRI scanner was used to produce a series of 1000 test images differing randomly in image noise, k-space phase scatter and object-to-background surface ratio. The outcome of each reconstruction was measured by extracting three parameters from the corrected image: the difference between the phase errors and the estimation, the amount of signal in the background and the shift of the object in the phase-encode direction after reconstruction.

The simulation used a Gaussian-distributed phase scatter among k-space lines of 0 to 120°, a Gaussian-distributed complex noise from 0.05 to 2% of the full scale of the FFT image, a threshold for the estimation of the background of 5 to 90% of the full scale of the image intensity and an object diameter of 100 to 20% of the image width. The algorithm was coded in Matlab 2014a and processed on an Intel Core i5-3470 CPU.

### 2.3. Reconstruction of experimental data

The optimal conditions of convergence found from the simulations were used to correct experimental images acquired on our FFC-MRI scanners. The images were acquired on the pre-clinical FFC-MRI scanner at 0.5 T using a 8 mm-thick cylindrical phantom of 5 cm diameter filled with 2 mM aqueous solution of $CuSO_4$ ($T_1$ = 350 ms at 0.5 T). For the 0.2 T whole-body FFC-MRI scanner the acquisition was performed at 0.2 T on a 10 cm-thick spherical Perspex phantom of 20 cm diameter containing 0.8 mM $MnCl_2$ in distilled $H_2O$ ($T_1$ = 110 ms at 0.2 T). All images were acquired using a Cartesian spin-echo sequence with an image size of 64 × 64, field of view of 230 mm, echo time of 22 ms and repetition time of 3 s.

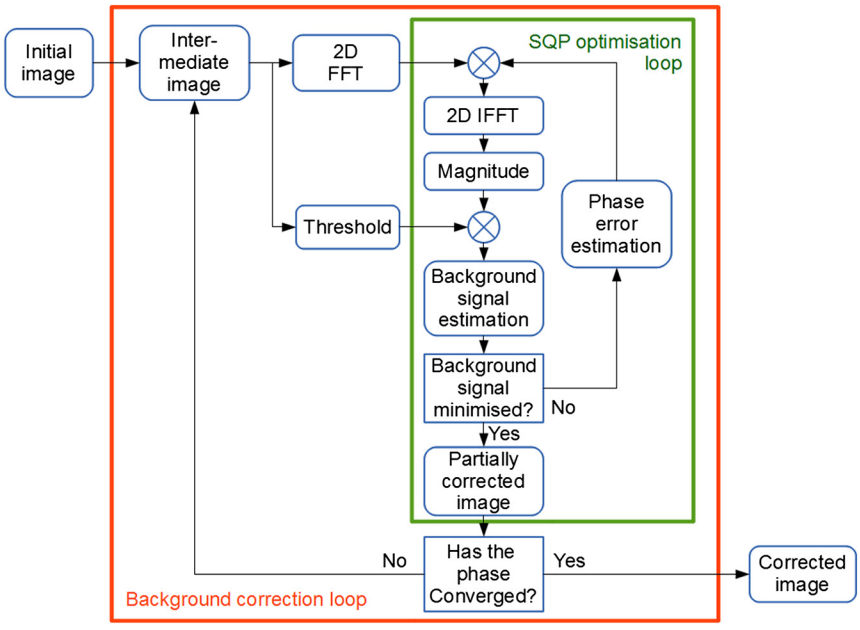


**Fig. 1.** Diagram of the correction algorithm. The input is a complex image, as obtained from the scan after a 2D Fourier Transform. The background is estimated in the red loop and remains unchanged during the SQP optimisation that estimates the phase error in the k-space. When an optimum phase error is found the complex image and the background are updated for the next iteration. The loop terminates when the phase error converges between two SQP iterations, or after the maximum number of iteration is reached. (For interpretation of the references to colour in this figure legend, the reader is referred to the web version of this article.)

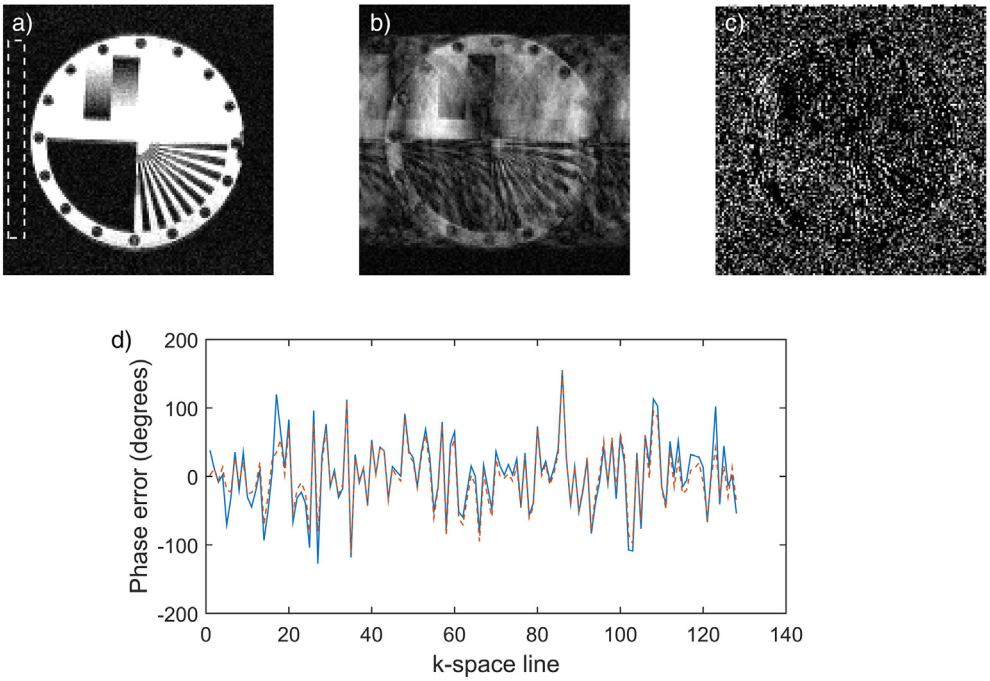


**Fig. 2.** Example of simulated image correction, with horizontal phase encoding direction. a) Reference 128 × 128 image selected from a stack of images acquired on a stable FFC-MRI scanner from previous quality control studies. The dashed lines delineate the signal-free region provided to the algorithm. b) Degraded image obtained by the addition of random phase along each phase-encode line of its k-space. c) Difference between the degraded and corrected images magnified 15 times. d) Comparison of the phase error injected in the k-space (plain) and its estimation (dashed). (For interpretation of the references to colour in this figure legend, the reader is referred to the web version of this article.)

## 3. Results

### 3.1. Simulations

Fig. 2 presents the reference image (a) together with a typical degraded image generated from the Monte-Carlo simulation (b) and the difference between the initial image and the corrected one (c). The phase encode direction is horizontal; no initial guess was provided in this case. The injection of phase scatter along phase-encoded k-space lines resulted in a ghosting in the phase-encoding direction, as expected, that was well corrected except for some boundaries that were slightly displaced. The graph in Fig. 2d compares the random phase error injected to produce the ghosted image (blue line) and its estimation by the algorithm (orange line): the estimation was good except at high special frequencies, which are generally underestimated as illustrated in that particular simulation. The average, maximum and minimum correction times per image were 8.0 s, 31.2 s and 0.9 s respectively for 64 × 64 images. 128 × 128 oversampled version of the test image took 7 s for correction, which increased to 104 s for 512 × 512 images. 47% of the calculations required less than five iterations to converge and about 0.1% required more than ten.

Fig. 3 and Fig. 4 show the effects of the scatter in the phase error injected in the image on the recovery of the phase error and on the signal that leaked into the background, with or without the use of an initial guess for the estimation of the background. Images with a scatter below about 50° RMS tended to be reconstructed well, but above this limit the outcome depended strongly on the object size. Images with small background tended not to be reconstructed well unless an initial guess was provided for the background. A minimum scatter of 2° in the corrected image was also observed even for low values of injected phase errors. Fig. 4 also shows that large phase scatter in k-space led to larger noise in the image regardless of the outcome of the reconstruction, though this unwanted effect could be drastically reduced by providing an initial guess for the background. Images with large objects tended to produce

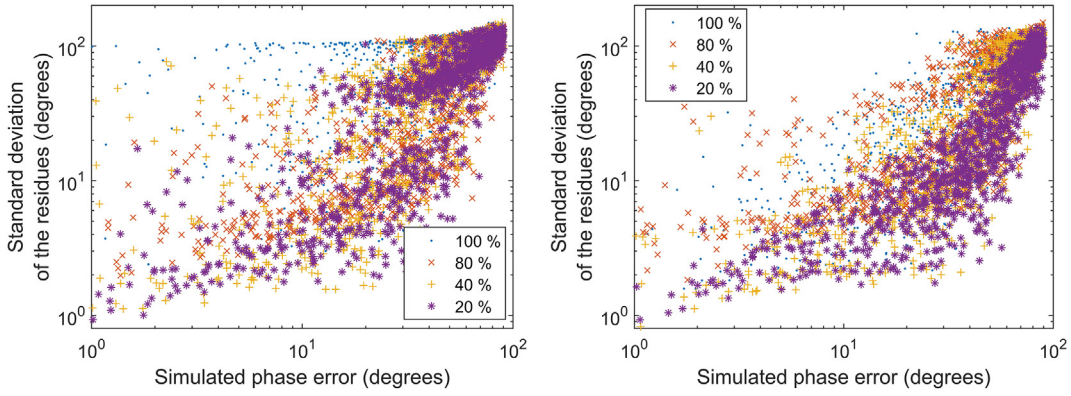


**Fig. 3.** Amplitude of the scatter in the residues of the phase estimation without (left) and with (right) the use of the initial guess for the background estimation. The different colours represent the diameter of the object compared with the image width. (For interpretation of the references to colour in this figure legend, the reader is referred to the web version of this article.)

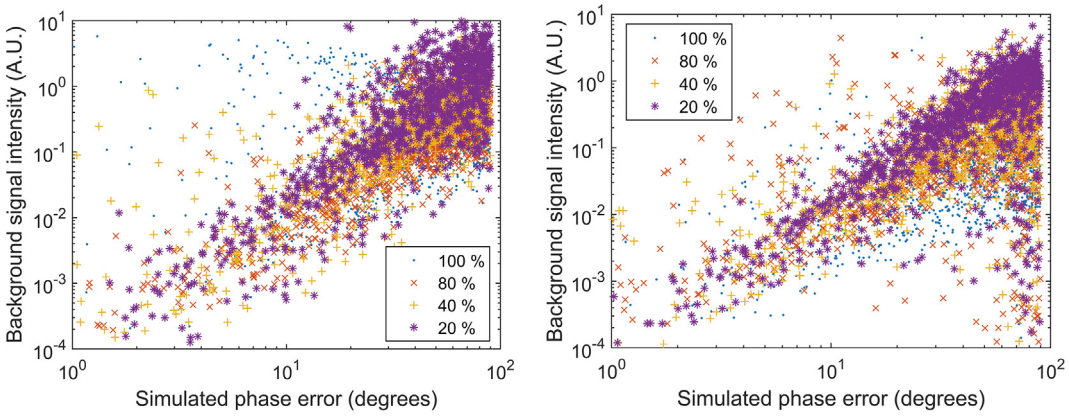


**Fig. 4.** Signal intensity in the background with the phase error injected without (left) and with (right) the use of an initial guess for the background estimation. The different colours represent the diameter of the object compared with the image width. (For interpretation of the references to colour in this figure legend, the reader is referred to the web version of this article.)

more noise after correction. When the phase error became larger than 70° RMS the correction algorithm also tended to shift the position of the object in the image due to the addition of a linear term in the phase correction array that wrapped around the ±180° limits so that it could not be detected by the algorithm. It should also be noted that algorithms other than SQP were tried: the Matlab minimisation function fmincon also offers 'trust-region-reflective' and 'interior-point' but neither of them could accurately determine the phase error over the high-frequency region of k-space.

### 3.2. Experimental data

The best reconstruction parameters obtained from the simulations were a background threshold of 0.2 and a background region of at least 20% of the image width in the phase-encode direction. We used these parameters to reconstruct experimental data from the 0.2 T and 0.5 T FFC-MRI systems (Fig. 5). The original 0.2 T image (Fig. 5a) showed a scatter in the phase-encode direction (horizontal) that disappeared after correction (Fig. 5b). The correction took a 2.9 s and makes it easier

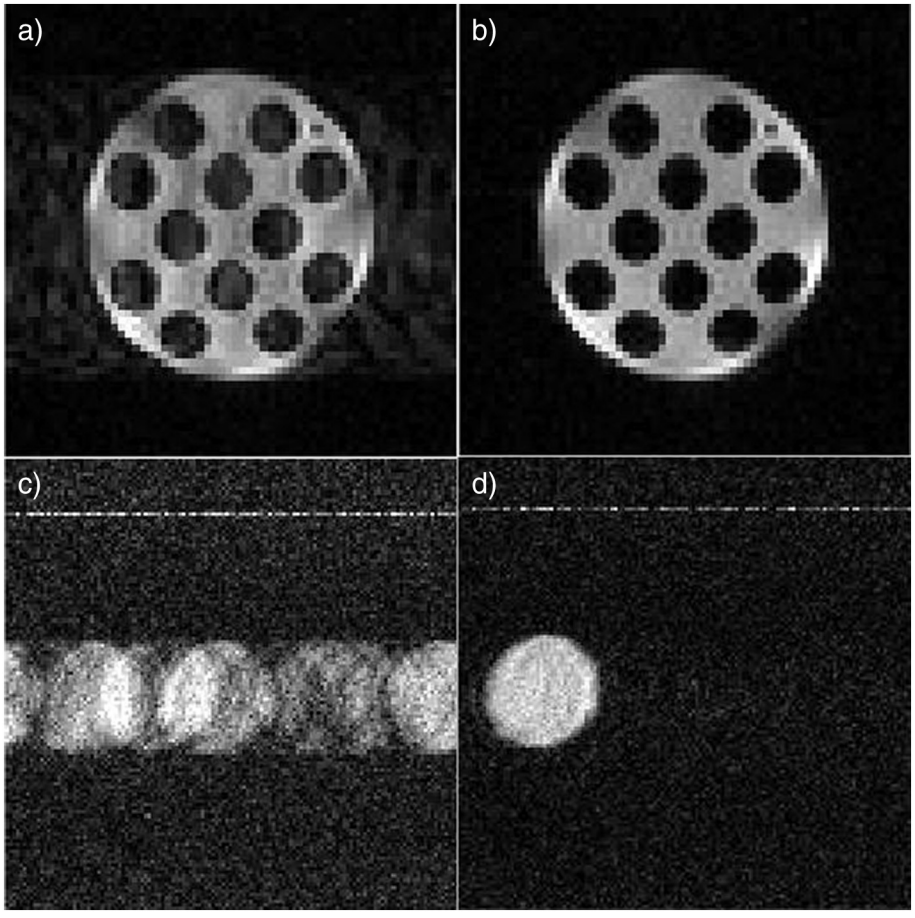


**Fig. 5.** a) Raw image acquired from a 0.2 T FFC-MRI scanner and b) Corrected version obtained in 2.9 s. c) Raw image of a cylindrical phantom acquired from a 0.5 T FFC-MRI scanner and d) Corrected version of image d obtained in 21 s.

to see a small distortion in the upper-left to lower-right direction which was subsequently adjusted. The random phase recovered by the algorithm did not show any time-dependant pattern and followed a Gaussian distribution of 25° standard deviation.

Images acquired on the 0.5 T system showed much stronger ghosting with a zipper artefact (Fig. 5c). The reconstruction still gave very good results (Fig. 5d) and corrected for all phase-encoding artefacts visible even though the noise scatter was estimated to be 82° so that corrections were larger than the limit estimated by the simulation, probably because the background region was very large. One can note that the zipper artefact still spread along the phase-encode direction after image correction indicating that its source was not synchronous with the acquisition and was therefore likely to be due to an external radiofrequency source. FFC-MRI scanners can easily correct for this problem by adjusting the acquisition field to shift RF artefacts out of the field of view.

## 4. Discussion

The algorithm proposed here has several limitations: the maximum phase scatter recoverable is 40° to 90° depending on the object size, the minimum phase scatter worth correcting is 2°, oversampling is required and the object may shift over the phase-encode direction. Fig. 3 shows clearly that image recovery is largely good below 20° RMS of phase scatter, and very unstable systems require large oversampling in the phase-encode direction to be corrected by this approach. In addition to this the algorithm generates a random de-phasing of 2° RMS minimum between the phase-encode lines even if very little noise is injected at the first place and so slightly degrades the quality of the image. Therefore images with less than 2° RMS errors should not be corrected. There is also a clear limitation in the oversampling ratio and at least 20% of the image should be background in order to allow for good corrections unless an initial guess can be provided (even a rough one). This oversampling requirement may be difficult to perform over regions internal to the body in which case one may spoil a band of the image in the phase-encode direction to produce a similar region. The reconstruction time is reasonable but increases exponentially with image matrix size. Finally, for very unstable systems, the object may shift in the phase-encode direction. This problem is mitigated by nulling the linear terms in the SQP algorithm and in practice we corrected this effect by using phase correlation image registration [14]. Despite these limitations, the algorithm proposed here allowed correcting for experimental data and was surprisingly robust on our 0.2 T FFC-MRI systems as it did not fail to converge on fifty images acquired experimentally. Corrections of images from the 0.5 T scanner do require some manual inputs but could also be corrected.

## 5. Conclusion

This work proved that the problem that affects the images acquired by our resistive FFC-MRI scanners is due to poor reproducibility between k-space line acquisitions but that no other problems are significantly affecting their performance for image quality. The ability to obtain a good estimation of the random phase error will allow us to better study its origins. This algorithm could probably be much improved: the SQP algorithm may not be the best option and parallelisable methods such as simulated annealing should be investigated; it would also be interesting to exploit the conjugate symmetry of the k-space phase map in order to reduce the number of correction parameters by a factor 2; additionally, we have so far restricted the correction algorithm to Cartesian acquisitions but other trajectories may be used with modifications. Finally it may be possible to apply this technique in other contexts such as motion artefact or random external sources of magnetic fields in order to compensate for effects that generate random phase errors in one direction of the k-space, with adaptations to fit the pulse sequence.

## References

[1] Lurie DJ, Aime S, Baroni S, Booth NA, Broche LM, Choi C-H, et al. Fast field-cycling magnetic resonance imaging. C R Phys Mar 2010;11(2):136–48.
[2] Anoardo E, Galli G, Ferrante G. Fast-field-cycling NMR: applications and instrumentation. Appl Magn Reson Apr 2001;20(3):365–404.
[3] Kimmich R, Anoardo E. Field-cycling NMR relaxometry. Prog Nucl Magn Reson Spectrosc Jul 30 2004;44(3–4):257–320.
[4] Kruk D, Herrmann A, Rössler EA. Field-cycling NMR relaxometry of viscous liquids and polymers. Prog Nucl Magn Reson Spectrosc May 2012;63:33–64.
[5] Korb J-P. Multi-scales nuclear spin relaxation of liquids in porous media. C R Phys Mar 2010;11(2):192–203.
[6] Stapf S, Ren X, Talnishnikh E, Blümich B. Spatial distribution of coke residues in porous catalyst pellets analyzed by field-cycling relaxometry and parameter imaging. Magn Reson Imaging Feb 2005;23(2):383–6.
[7] Koenig SH, Brown III RD. Field-cycling relaxometry of protein solutions and tissue: implications for MRI. Prog Nucl Magn Reson Spectrosc 1990;22(6):487–567.
[8] Broche LM, Ashcroft GP, Lurie DJ. Detection of osteoarthritis in knee and hip joints by fast field-cycling NMR. Magn Reson Med 2012;68(2):358–62.
[9] Broche LM, Ismail SR, Booth NA, Lurie DJ. Measurement of fibrin concentration by fast field-cycling NMR. Magn Reson Med 2012;67(5):1453–7.
[10] Miller KL, Pauly JM. Nonlinear phase correction for navigated diffusion imaging. Magn Reson Med Aug 2003;50(2):343–53.
[11] Atkinson D, Hill DL, Stoyle PN, Summers PE, Keevil SF. Automatic correction of motion artifacts in magnetic resonance images using an entropy focus criterion. IEEE Trans Med Imaging Dec 1997;16(6):903–10.
[12] McGee KP, Manduca A, Felmlee JP, Riederer SJ, Ehman RL. Image metric-based correction (autocorrection) of motion effects: analysis of image metrics. J Magn Reson Imaging Mar 2000;11(2):174–81.
[13] Schittkowski K. NLPQL: a fortran subroutine solving constrained nonlinear programming problems. Ann Oper Res Jun 1986;5(2):485–500.
[14] Reddy BS, Chatterji BN. An FFT-based technique for translation, rotation, and scale-invariant image registration. IEEE Trans Image Process Aug 1996;5(8):1266–71.